DENTAL MATERIALS 34 (2018) 1112–1126

Available online at www.sciencedirect.com

ScienceDirect

journal homepage: www.intl.elsevierhealth.com/journals/dema

In vitro and *in vivo* studies of anti-bacterial copper-bearing titanium alloy for dental application

Rui Liu[a,b,1], *Yulong Tang*[c,1], *Lilan Zeng*[d], *Ying Zhao*[d], *Zheng Ma*[a], *Ziqing Sun*[a], *Liangbi Xiang*[e,*], *Ling Ren*[a,*], *Ke Yang*[a]

[a] *Institute of Metal Research, Chinese Academy of Sciences, 72 Wenhua Road, Shenyang 110016, China*
[b] *Northeastern University, 3-11 Wenhua Road, Shenyang 110819, China*
[c] *Department of Stomatology, General Hospital of Shenyang Military Area, Shenyang 110016, China*
[d] *Center for Human Tissues and Organs Degeneration, Shenzhen Institute of Advanced Technology, Chinese Academy of Science, Shenzhen 518055, China*
[e] *Department of Orthopedics, General Hospital of Shenyang Military Area, Shenyang 110016, China*

ARTICLE INFO

Article history:
Received 25 December 2017
Received in revised form
12 April 2018
Accepted 15 April 2018

Keywords:
Dental implants
Titanium
Copper
Anti-bacterial
Biofilm
Peri-implantitis

ABSTRACT

Objective. A novel copper-bearing titanium alloy (Ti–Cu) was fabricated for dental application that is expected to efficiently restrain the growth of bacteria and discourage biofilm formation. The aim of this study was to investigate both the antibacterial activity and biofilm inhibition of Ti–Cu alloy *in vitro*, and the antibacterial effect of Ti–Cu implant in early stage of peri-implantitis *in vivo*.

Methods. *Staphylococcus aureus* and *Escherichia coli* were selected to evaluate the antibacterial activity of Ti–Cu alloy and Ti served as control. The antibacterial rate, attached bacteria and developed biofilms were studied from quantitative antibacterial test, biofilm observation and bacterial morphological examination. Electrochemical tests were used to investigate the corrosion property of Ti–Cu alloy. Furthermore, both Ti and Ti–Cu dental implants were manufactured and then implanted in the mandibular premolar sites of beagle dogs for 3 months with ligature-infected treatment. Implant-tissue samples were prepared for radiographic analysis, Micro-CT evaluation and histological examination.

Results. Ti–Cu alloy was found to efficiently kill the attached bacteria by ways of damaging cell membranes and cell walls and strongly inhibit the biofilm formation. However, Ti–Cu alloy had excellent corrosion resistance similar with Ti. Further, Ti–Cu dental implants showed superior capacities of inhibiting the bone resorption caused by bacterial infection and enhancing bone formation.

* *Corresponding authors.*
E-mail addresses: xiangliangbi1963@sina.com (L. Xiang), lren@imr.ac.cn (L. Ren).
[1] These authors contributed equally to this work.
https://doi.org/10.1016/j.dental.2018.04.007

Significance. Ti–Cu alloy strongly inhibited biofilm formation *in vitro* and prevented bacterial infection associated with dental implant *in vivo*, making it great potential for application in dental implants with excellent antibacterial viability and positive effect against bone resorption induced by peri-implantitis.

1. Introduction

Titanium (Ti) and its alloys are extensively applied in clinic as preferred metallic medical materials due to their excellent combination of mechanical properties, corrosion resistance and biocompatibility [1]. However, titanium and its alloys are inert materials in biological environment, *i.e.*, they have less bioactive functions, such as antimicrobial activity, promotion of osteogenesis, *etc.* [2]. It has been known that the adherence and colonization of bacteria on the surface of implants can lead to formation of biofilm, a firm layer composed of bacteria with the secreted glycoproteins and polysaccharides, which can cause infection and inflammation like peri-implantitis probably resulting in the failure of implantation [3]. Peri-implantitis inflammatory reactions have been detected in about 10% to 45% of dental implants within 10 years after implantation [4]. Therefore, peri-implantitis remains a persistent clinical problem without an easy treatment. It is an instinctive reaction for the bacteria to adhere on the surface and then form a biofilm for self-protection, which is a cycling dynamic process [5]. An important characteristic of bacterial biofilms is their innate resistances to both immune system and antibiotics [6,7]. Resistance to antibiotics of the bacteria in a biofilm may improve 10–1000 times compared with that of planktonic bacteria [8]. It has been estimated that over 60% of bacterial infections currently treated in hospitals are caused by the bacterial biofilm [5]. Therefore, by inhibiting the formation of biofilm on the surface of implant, it should be an effective way to control the implant-associated infection including peri-implantitis.

Copper (Cu) has long been known as a necessary trace element in the human body, and shows excellent biological properties, such as anti-inflammatory, anti-microbial and anti-proliferative properties [9]. Previous researches have confirmed the favorable antibacterial ability of copper-containing coatings. Li et al. prepared a Cu-containing bioactive glass nano-coating with uniform nanostructure on natural eggshell membrane (Cu-BG/ESM) that improved osteogenesis, angiogenesis and antibacterial activities of the material [10]. A Ti–Cu coated layer on 316L stainless steel (316L-SS) was fabricated to improve the antibacterial activity, corrosion and tribological properties [11]. Longevity and safety, however, are the main concerns for clinical adoption [7]. Bacterial contamination may occur not only peri-operatively but also hematogenously later during the life time of the implant [12,13]. This problem cannot be circumvented by coating with a releasing strategy because the antibacterial agent or antibacterial ions in the coating would run out eventually [14]. Therefore, it is of vital importance to develop the integral antibacterial materials by immobilizing antibacterial agent into materials for long-term effective antibacterial activity. A proper incorporation of Cu into stainless steel through the material melting has been reported to be an effective way to develop the integral antibacterial stainless steels with excellent antibacterial activity [15,16].

Meanwhile, there have some studies in terms of antibacterial Ti–Cu sintered alloys with the microstructure of β-transform phase [17,18]. However, the plasticity of the above Ti–Cu alloys would be not enough to machine dental implant and then difficult to gain application in clinic. Considering this, equiaxed α phase Ti–Cu alloys with optimized microstructure and mechanical property were obtained after optimizing heat treatment. Based upon this work, our previous *in vitro* study [19] proved that Ti–Cu had antibacterial and anti-biofilm ability against oral bacterial strains of *Porphyromonas gingivalis* (*P. gingivalis*) and *Streptococcus mutans* (*S. mutans*). Consequently, the aim of the present work was to further and systematically evaluate the antimicrobial activity of Ti–Cu alloy from both *in vitro* and *in vivo* tests. Various properties were assessed *in vitro* by using *Staphylococcus aureus* and *Escherichia coli*, including bacteria adhesion, cell morphological change, structure and viability of the biofilm on Ti–Cu alloy as well as the antibacterial activity. In addition to this, Ti–Cu implants were fabricated and a modified peri-implantitis dog model was established in order to evaluate the antibacterial activity of Ti–Cu alloy dental implant *in vivo* by means of X-ray, Micro-CT and histological assessment.

2. Material and methods

2.1. Material preparation

A Ti–Cu alloy with 5 wt.% Cu content was prepared in a vacuum consumable furnace from high purity Ti and Cu. The ingot was initially re-melted three times and hot forged to bar with 40 mm in diameter and then heat treated at 850 °C for 2 h followed by cooling in furnace.

For Cu ion release test and *in vivo* bacterial-related tests, including quantitative antibacterial test, SEM observation, biofilm staining assay and TEM observation, Ti–Cu alloy and commercially pure Ti were machined to small samples with diameter of 10 mm and thickness of 2 mm. Samples were further ground with SiC paper up to 2000 grit, washed by acetone, ethanol and sterile deionized water, dried by warm air, and finally disinfected by ultraviolet light prior to experiments.

Samples for electrochemical tests were cut with diameter of 10 mm and thickness of 5 mm and linked up with a copper wire at the back. Every sample was put into a polymer sample holder with only one side of 20 mm in diameter exposed and then mounted in epoxy resin that covered the entire back. Before test, samples need to be polished with SiC paper up to

2000 grit, and ultrasonically cleaned with acetone, ethanol and sterile deionized water successively.

2.2. *In vitro tests*

2.2.1. *Bacterial culture*

Considering the wide clinic applications of Ti–Cu such as orthopedics, the two classic strains of implant associated infections, *Staphylococcus aureus* (*S. aureus*, ATCC 25923) and *Escherichia coli* (*E. coli*, ATCC 25922), provided by Guangzhou Institute of Microbiology, China, are chosen in this article to evaluate the antibacterial ability of Ti–Cu. The strains were cultured in LB medium (5 g/l beef extract, 10 g/l peptone and 5 g/l NaCl, pH 7.2–7.4) and LB agar plates (20 g/l LB medium and 20 g/l agar powder). A series of bacterial suspensions with concentrations of 10^3–10^8 CFU/ml using sterile PBS buffer or LB medium were prepared for experiments.

2.2.2. *Quantitative antibacterial test*

According to ISO 10993-5: 2009 standard, the contacting test was conducted to evaluate the antibacterial and anti-biofilm abilities of the Ti–Cu alloy [20]. A drop (50 μl) of bacterial suspension with a concentration of 10^6 CFU/ml was put onto the surface of the samples including Ti as the control group and the experimental Ti–Cu alloy group. After culturing at 37 °C and 90% relative humidity for 2, 6, 12 and 24 h, the samples with the suspension were vortexed with 2 ml sterile PBS buffer sufficiently. After that, 50 μl of the washed liquid was spread onto the counting agar plates and then incubated at 37 °C for 24 h at least. Then these plates were photographed and bacterial colony number was counted. Finally, the bacterial concentration on the samples after co-culture (N, CFU/ml) was calculated by Eq. (1) while the antibacterial rate (R) by Eq. (2) [21], $R \geq 99\%$ meaning strong antibacterial activity and $R \geq 90\%$ antibacterial activity.

$$N = C \times d \times 1000/l \quad (1)$$

$$R = (N_{control} - N_{material})/N_{control} \times 100\% \quad (2)$$

In Eq. (1), C means average colony count in the plates, d means dilution factor and here $d = 41$, while l is the volume of the bacterial suspension on the samples and here $l = 50$. In Eq. (2), $N_{control}$ and $N_{material}$ are the average colony counts for the control (Ti) and Ti–Cu samples, respectively. Three samples were used in this experiment (n = 3).

2.2.3. *SEM observation*

Ti–Cu alloy and Ti as control were incubated with 800 μl bacterial suspension (10^6 CFU/ml). After incubation for various time points, the samples with biofilm formation were lightly rinsed three times in PBS, fixed with glutaraldehyde (2.5% v/v) at 4 °C overnight, washed with PBS, and then dehydrated in a series of ethanol solutions (50%, 60%, 70%, 80%, 90%, 95% and 100%) for 10 min each. Finally the samples were dried at room temperature for 24 h at least and sputtering-coated with gold. The biofilms were observed on a scanning electron microscope (SEM, Phillips XL30FEG, Netherlands). Three samples were used in this experiment (n = 3).

2.2.4. *Bacteria dead/live assay*

To further analyze the viability of the adhered bacteria and the formation of biofilm on the surfaces, the LIVE/DEAD Bacterial Viability Kit (Invitrogen Inc., USA) was used, which included two stains, SYTO-9 labeling live cells green whereas PI (propidium iodide) labeling dead cells red. Prior to staining, Ti–Cu alloy and Ti as control were incubated with 800 μl bacterial suspension (10^7–10^8 CFU/ml) for 24 h. According to the specification, the biofilm formed on samples was washed thrice by PBS and then stained with 50 μl of the mixed staining solution (SYTO-9:PI:PBS = 3:3:1000) for 15 min in darkness. Afterwards, the samples were observed under a confocal laser scanning microscopy (CLSM, Olympus FV10-ASW, Japan) and the images were obtained with a ×20 objective. The images were then quantitatively analyzed using the software ImageJ and three-dimension imaging was reconstructed by using the NIS Viewer software. Three samples were used in this experiment (n = 3).

2.2.5. *Fluorescence microscopy*

The fluorescence microscopy technique was implemented to investigate surface coverage by bacteria and EPS (both proteins and polysaccharides). After biofilm developed on the surfaces of Ti and Ti–Cu for 24 h, surfaces were stained with DAPI (4′,6-diamidino-2-phenylindole), SYPRO tangerine, and Alexa 633 conjugated concanavalin A (ConA-Alexa 633), respectively. To remove planktonic cells and loosely-attached biofilms, the samples need to be rinsed with PBS initially. Then, they were stained with DAPI (50 μl of 1 mg/ml stock solution) for 15 min in dark. Next ConA (50 μl of 0.05 mg/ml solution) was used to stain polysaccharides for another 15 min in dark. Subsequently, samples were stained with SYPRO tangerine (50 μl of 50 μl/ml solution) to label the protein portion of the EPS. The samples were gently rinsed in PBS after each step. After staining, fluorescence micrographs were taken to obtain images. Surface coverage data was extracted from the images and quantitatively analyzed using ImageJ software. Three samples were used in this experiment (n = 3).

2.2.6. *TEM observation*

Transmission electron microscope (TEM) was used to examine the intracellular changes in the two bacterial strains. After 24 h of co-culture, the biofilm formed on samples were washed twice with PBS and then centrifuged at 3000 rpm for 5 min. The pellets were separately fixed with 2.5% v/v glutaraldehyde at 4 °C for at least 2 h. The samples were then washed with dimethyl sodium arsenate buffer three times and the pellets were fixed in 1% (wt/vol) osmium tetroxide (OsO_4) at 4 °C for 1.5 h. Cells were then dehydrated with an ascending concentrations of ethyl alcohol (50%, 70%) and acetone (80%, 90% and twice of 100%) for 15 min each. Dehydrated samples were then embedded in paraffin wax and thin sections (approximately 60 nm) were cut using an ultramicrotome (PowerTome-PC; RMC, USA). These obtained sections were sequentially placed on the copper net and stained with 4% uranyl acetate and Reynolds' lead citrate. Finally the samples were viewed on a TEM (TECNAI G2, Electron Optics, USA) at 80 kV in high-vacuum mode. This experiment was carried out in triplicate (n = 3).

2.3. Electrochemical test

The potentiodynamic polarization curve was measured at 37 ± 0.5 °C on an Autolabpotentiostat-galvanostat (Reference 600, Gamry Instruments Inc., USA). The samples were put as the working electrode and a platinum plate electrode (10 mm × 10 mm × 1 mm) was used as the counter electrode, and the saturated calomel electrode (SCE) was used as the reference electrode. Working electrode and electrolyte (0.9% (m/v) NaCl solution with pH 7.2, used to simulate the human body fluid) were renewed before start of tests and all the samples were tested after the E_{OCP} was stabilized. Potentiodynamic measurements were performed at a scanning rate of 0.5 mV/s starting from −0.5 V to 2.0 V (SCE). Each test was conducted for three times (n = 3).

2.4. Cu ion release

According to the ISO 10993-12 standard [22], the Cu^{2+} released from Ti–Cu alloy for various periods of time was monitored in 0.9% NaCl solution at 37 °C with a ratio of solution/sample surface area of 1.25 cm^2/ml. The concentrations of released Cu^{2+} of each harvested sample at 2, 6, 12 and 24 h were determined by inductively coupled plasma mass spectrometry (ICP-MS, Thermo, USA). Three samples were used for every time point in this experiment (n = 3).

2.5. In vivo tests

2.5.1. Implant preparation

Ti–Cu dental implants with 3.5 mm in diameter and 10 mm in length were successfully machined according to the design as shown in Fig. 1a, which is the first Ti–Cu alloy dental implant in the world as shown in Fig. 1b. Meanwhile, Ti implants as control were also machined as per the Ti–Cu implant. Then, all the implants were orderly cleaned with acetone, deionized water and ethyl alcohol under ultrasonic condition. Each implant was individually packaged, sterilized with ethylene oxide and stored at room temperature. Eight implants were used in this experiment (n = 8).

2.5.2. Surgical procedures

The experimental protocol was approved by the Animal Care Committee, General Hospital of Shenyang Military Area. The subjects were 4 male beagles (1-year-old, 13–16.5 kg). Each underwent bilateral extraction of mandibular premolars and first molars. Three months later, each dog had 2 implants placed on each side of the mandible in the healed extraction sites. After sedation with acepromazine (0.17 mg/kg

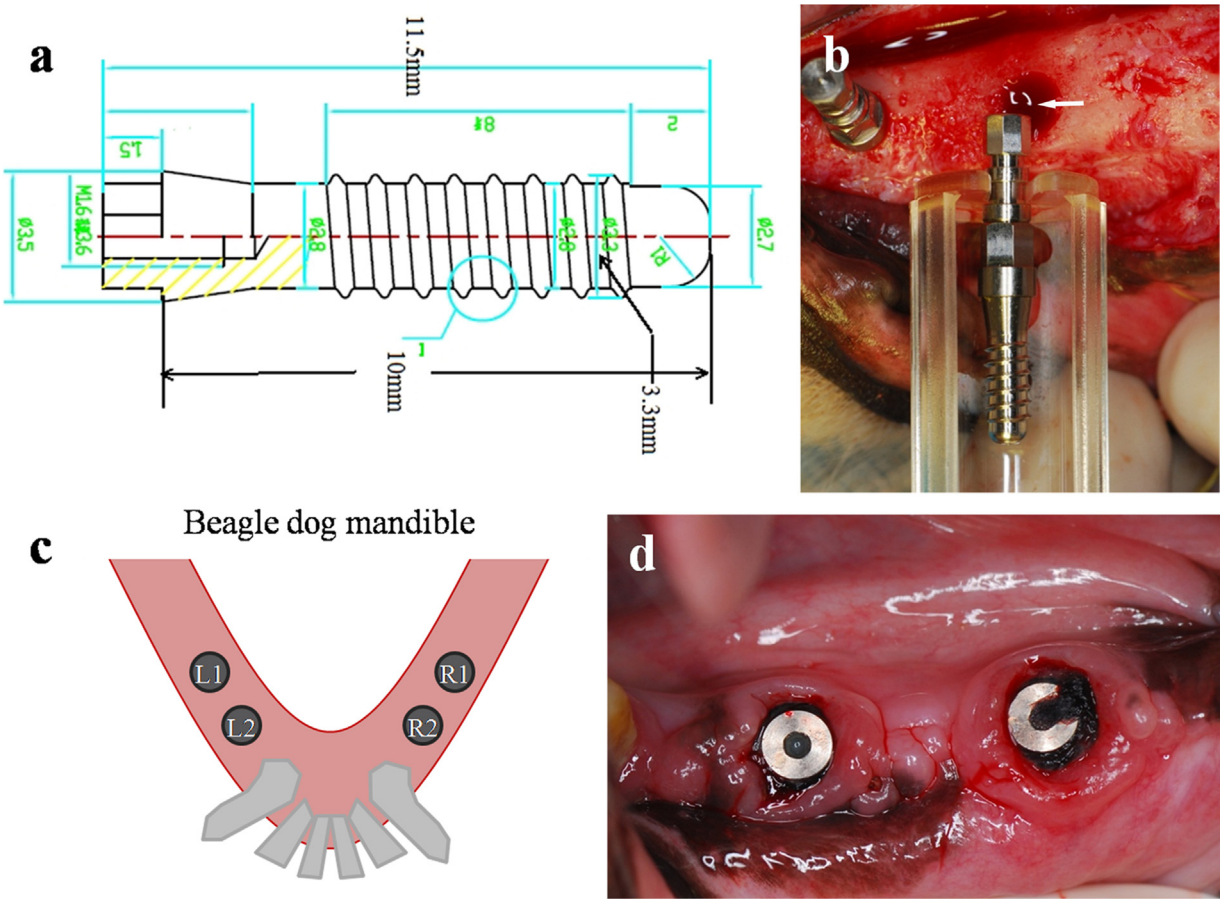

Fig. 1 – Experimental design for *in vivo* animal tests: (a) implant device: screw-shaped Ti implant, diameter of 3.5 mm, length of 10 mm; (b) clinical photograph illustrating the implants used in the study; (c) dog mandible diagram: L1–L2 and R1–R2 are the left- and right-mandible implant sites; (d) clinical situation after the implantation and ligature-induced treatment, two implants were installed on each side of the mandible.

body weight), the dogs were anesthetized with 21.5 mg/kg thiopental-sodium. For all the surgical procedures, inhalation anesthesia was administered using oxygen and nitrous oxide and isoflurane. A full-thickness flap was elevated, and four external hexed and screw-type custom-made implants, 3.5 × 10 mm with a 1.8 mm high collar segment, were inserted into the edentulous area on each side (Ti in left, Ti–Cu in right, marked as Fig. 1c). Implants were placed by using a standard method and each was implanted to a similar depth with the coronal margin at the level of the alveolar bone crest (Fig. 1b). Each implant was connected with a 3-mm custom-made abutment and flaps were sutured through the abutments. Then, on each side of the mandible, cotton floss ligatures were placed around the abutments (Fig. 1d) to promote plaque accumulation and induce plaque-associated peri-implant inflammation according to a method described previously [23,24]. Ligatures were secured apically to the prominence of the abutment, maintaining contact with the peri-implant mucosal margins for 3 months. Meanwhile, a high-sugar soft diet (500 g/per dog/day) was made after surgery. Dogs were sacrificed 3 months after ligature placement by an intravenous lethal overdose of sodium pentobarbital injection. Mandible tissue blocks were separated and immersed in 10% formalin.

2.5.3. *Radiographic analysis*

In the beginning and 3 months after the surgery, sets of radiographs were obtained respectively. The radiographs were analyzed using an Olympus SZH10 stereo macroscope (Olympus, Tokyo, Japan) and digital images were obtained with a Leica DFC280 camera (Leica, Wetzlar, Germany). The vertical distance from the implant shoulder to the marginal bone level was assessed at the mesial and distal aspects of each implant using the QWin software (Leica Qwin Standard V3.2.0, Leica Imaging Systems Ltd., Cambridge, UK). Three months after implantation, the experimental peri-implantitis was initiated.

2.5.4. *Micro-CT*

After the mandibles were removed and stored in the fixative, the implants were scanned by local micro-computed tomography (Inveon, Siemens, Germany) at a scanning resolution of 14.97 μm to evaluate the changes in peri-implant tissue including trabecular thickness (Tb.Th), trabecular number (Tb.N), trabecular separation (Tb.Sp), bone surface/bone volume (BS/BV), and bone volume/total volume (BV/TV). The regions of interest, including the trabecular compartment around implant, were selected. The trabecular compartment region was defined as a ring with a radius of 0.5 mm from the implant surface.

2.5.5. *Histomorphometric and histological analysis*

After Micro-CT imaging, the specimens were immersed in 10% buffered formalin solution at room temperature (25 °C). Then the tissue blocks containing the implant and the surrounding soft and hard tissues in a mesial-distal direction were dissected using a diamond saw (Exakts, Kulzer, Germany) and processed for ground sectioning according to the methods described by Donath and Breuner [25]. Subsequently each implant in the blocks was sectioned in the bucco-lingual plane and two sections of each implant were prepared. All the sections were reduced to a thickness of 20–30 μm by grinding and polishing using a micro-grinding unit (Exacts Cutting, System, Apparatebau Gmbh, Germany) and stained by a Masson's trichrome staining kit. The histological examinations were performed using a camera with 1× magnification and a Leica DM-RBE microscope (Leica, Heidelberg, Germany) with 100× magnification. The bone-implant contact (BIC, %) ratio and bone resorption values were identified and used for the linear measurement [26]. BIC was calculated as the ratio of the length of the implant profile in direct contact with the bone surface to the total length of the implant profile. Bone resorption ratio was calculated as the ratio of the length of the bone resorption to the total length of the implant profile.

2.6. *Statistical analysis*

All the experiments were carried out in triplicate and three parallel samples were performed in every experiment (n = 3) except for the *in vivo* tests (n = 8). For each set, the relevant data was summarized as the mean standard deviation. Statistical significance was determined using SPSS 13.0 (SPSS Inc., Chicago, IL). The results were considered statistically significant at $^{*}p \leq 0.05$, $^{**}p \leq 0.01$ and $^{***}p \leq 0.001$.

3. Results

3.1. *Antibacterial activity*

Fig. 2a shows the bacterial colony growth on the surfaces of the Ti–Cu alloy and the control Ti after culturing with bacteria for 2, 6, 12 and 24 h. Fig. 2b and c represents the exact concentration (CFU/ml) of the bacteria on different samples at corresponding culturing time points as shown in Fig. 2a. Fig. 2b shows the concentration of *S. aureus* at different culturing time points. The concentration of alive *S. aureus* on the surface of Ti maintained around 7×10^5 CFU/ml before 6 h and decreased slightly to 6×10^5 CFU/ml from 6 h to 24 h. While the concentration of *S. aureus* on the surface of Ti–Cu alloy decreased sharply within 24 h as shown in Fig. 2b from 7×10^5 CFU/ml to 3.5×10^3 CFU/ml. The same situation occurred for *E. coli* as shown in Fig. 2c. The results of Fig. 2b and c indicated that after 24 h co-culture, the CFU counts for Ti were at least 2 logs more than Ti–Cu towards either *S. aureus* or *E. coli*. Meanwhile, the antibacterial rate of Ti–Cu alloy at various co-culturing time points are plotted in Fig. 2d. The Ti–Cu alloy has already presented certain antibacterial effect at 6 h with antibacterial rates of 72% and 69% against *S. aureus* and *E. coli*, respectively. Moreover, at 12 h, the antibacterial rates achieved to 80% and 96% respectively against two species. Finally at 24 h, the antibacterial rates against both *S. aureus* and *E. coli* all reached up to 99%. The above results indicated that Ti–Cu alloy possessed satisfied antimicrobial activity against both *S. aureus* and *E. coli*.

3.2. *Biofilm formation*

Photos of adhered bacteria on the surfaces of Ti and Ti–Cu alloy at certain culturing time points are shown in Fig. 3. Numerous bacteria adhered on the surface of Ti and the amount was increasing from 2 h to 24 h, then the biofilm was formed finally.

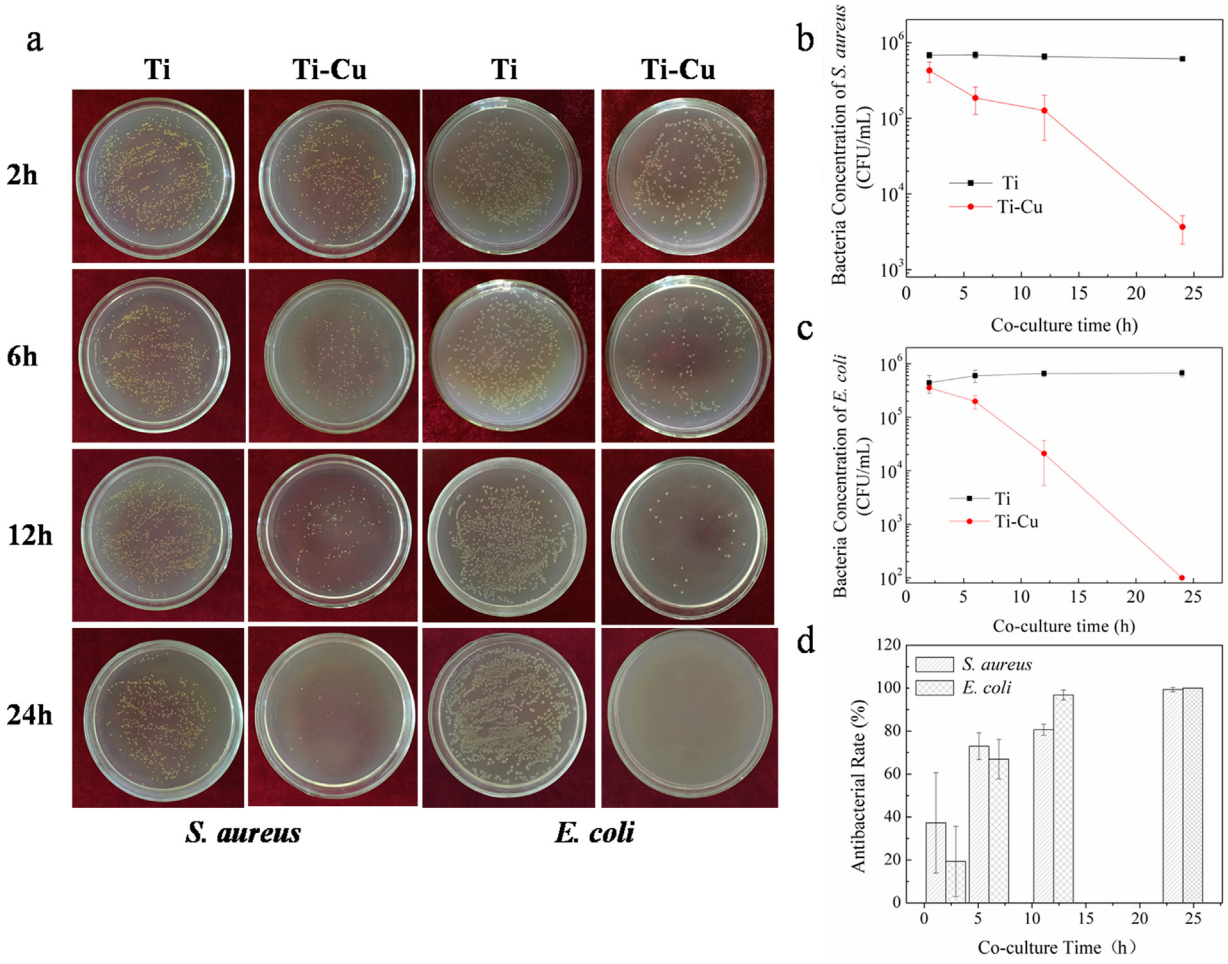

Fig. 2 – Antibacterial effects of materials co-cultured with *S. aureus* and *E. coli* for 2, 6, 12 and 24 h, respectively: (a) typical bacteria colonies on Ti and Ti–Cu for 2, 6, 12 and 24 h; (b) dependence of *S. aureus* concentration on the reaction time with Ti and Ti–Cu respectively; (c) dependence of *E. coli* concentration on the reaction time with Ti and Ti–Cu respectively; (d) antibacterial rates of Ti–Cu alloy against *S. aureus* and *E. coli* respectively.

However, only scattered bacteria on the surface of Ti–Cu could be observed during the whole culture time of 24 h. Meanwhile, there was no trend of biofilm formation on the surface of Ti–Cu. Consequently, Ti–Cu could reduce the adhesion of bacteria on its surface, no matter *S. aureus* or *E. coli*.

Fig. 4 shows the cell morphology observed by SEM with higher magnification. The *S. aureus* and *E. coli* cells on the surface of Ti had normal and complete morphologies (Fig. 4a and c, white arrows indicating normal cells and black arrow indicating intercellular substance), while some cells on the surface of Ti–Cu were abnormal. For instance, some bacteria were shriveled as arrowed in Fig. 4b and some were disappearing as arrowed in Fig. 4d.

3.3. *Bacterial viability*

Fig. 5 shows dead/live bacteria staining on the surfaces of Ti and Ti–Cu alloy. In order to further examine the biofilm formation, bacteria suspension with a high concentration were used to promote the adherence on the surface of the samples. In Fig. 5a, there was a large amount of viable bacteria stained as green on Ti surface but a minor quantity of green staining was observed on Ti–Cu alloy compared with Ti. Significant increase of dead bacterial count (red) was visualized on the surface of Ti–Cu as compared to Ti for both *S. aureus* and *E. coli*. The numbers of sessile live and dead cells were quantified from the average of 10 sets of CLSM images using the ImageJ software as shown in Fig. 5b and c, and the results are in agreement with the above conclusion.

A NIS-Elements viewer software was used to perform the three-dimensional reconstruction, and the reconstruction graphs are shown in Fig. 5a, which further supports the results from the above CLSM observations. In Fig. 5d, *S. aureus* biofilm formed on Ti exhibited a thickness of 18 μm, whereas 16 μm on the Ti–Cu surface. More obvious result was that *E. coli* biofilm formed on Ti exhibited a thickness of 24 μm, however 10 μm on Ti–Cu surface.

3.4. *EPS (both proteins and polysaccharides) in biofilm*

To investigate surface coverage by bacterial cells and EPS (both proteins and polysaccharides) in the biofilm, samples with

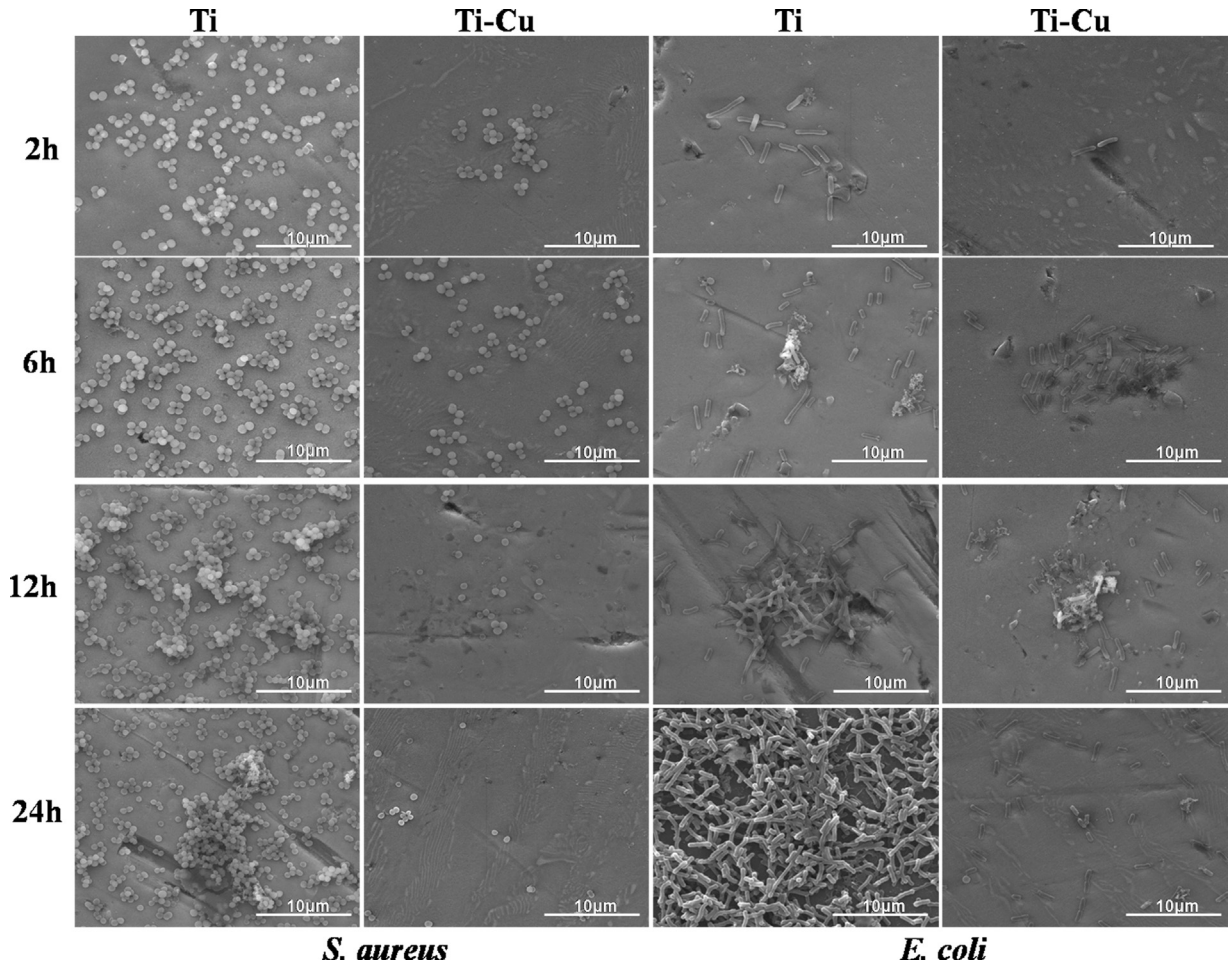

Fig. 3 – SEM morphologies of *S. aureus* and *E. coli* on surfaces of Ti and Ti–Cu alloy after co-cultured for 2, 6, 12 and 24 h.

biofilm were examined by a fluorescence microscope. And the results are listed in Fig. 6. It revealed that the formation of biofilm is heterogenous and the level of surface coverage by biofilms is different between Ti and Ti–Cu. It is obvious that the biofilms formed on Ti are more populous of the cells and the associated EPS is more massive. While, the polysaccharide and protein contents of the biofilm on Ti–Cu surface is lower than that of Ti. Furthermore, *S. aureus* biofilms covered the Ti surface to a higher extent (16% surface coverage for bacteria, 8% surface coverage for polysaccharides and 9% surface coverage for proteins) compared to Ti–Cu (4% surface coverage for bacteria, 1% surface coverage for polysaccharides and 0.4% surface coverage for proteins). And *E. coli* biofilms covered the Ti surface to a higher extent (31% surface coverage for bacteria, 20% surface coverage for polysaccharides and 14% surface coverage for proteins) compared to Ti–Cu (4% surface coverage for bacteria, 1.6% surface coverage for polysaccharides and 0.5% surface coverage for proteins).

3.5. *Morphological change*

In order to further confirm the antimicrobial ability and analyze the antibacterial mechanism, individual bacteria cultured for 24 h on the surface of samples were observed by means of TEM. There were no cell membrane change and any notable rupture for *S. aureus* after co-cultured with Ti as shown in Fig. 7a (indicated by white arrow), and meanwhile the cells clearly showed unanimous electron density, suggesting that the cells were in a healthy and normal condition. In contrast, *S. aureus* morphology changed remarkably after incubated on the surface of Ti–Cu alloy, as shown in Fig. 7b–d. Fig. 6b demonstrates that the bacterial cellular contents released into the surroundings and hence led to lower electron density as indicated by red arrow. Meanwhile, messy distributed electrons around the broken cells were also obviously observed as indicated by arrows. In other cells, the cell walls were seriously damaged with irregular cell shape and fuzzy boundary as arrowed in Fig. 7c. As described in Fig. 7d, *S. aureus* on the surface of Ti–Cu was shrinking, and cytoplasm membranes have been separated from the cell wall as arrowed in Fig. 7d.

Similar morphological changes of *E. coli* also appeared. Cells with the normal cytoplasm membrane of *E. coli* co-cultured with Ti are shown in Fig. 7e, and cells with Ti–Cu alloy are shown in Fig. 7f–h. Some tightly condensed substances are clearly visible in the center of the electron-light region (Fig. 7f) after co-cultured with Ti–Cu alloy. They were twisted together in the center of the electron-light region, like a twisted string. Meanwhile, cell cytoplasm membrane appeared to be detached from the cell wall as arrowed in Fig. 7f. In Fig. 7g, the cell walls were dissolved and damaged together

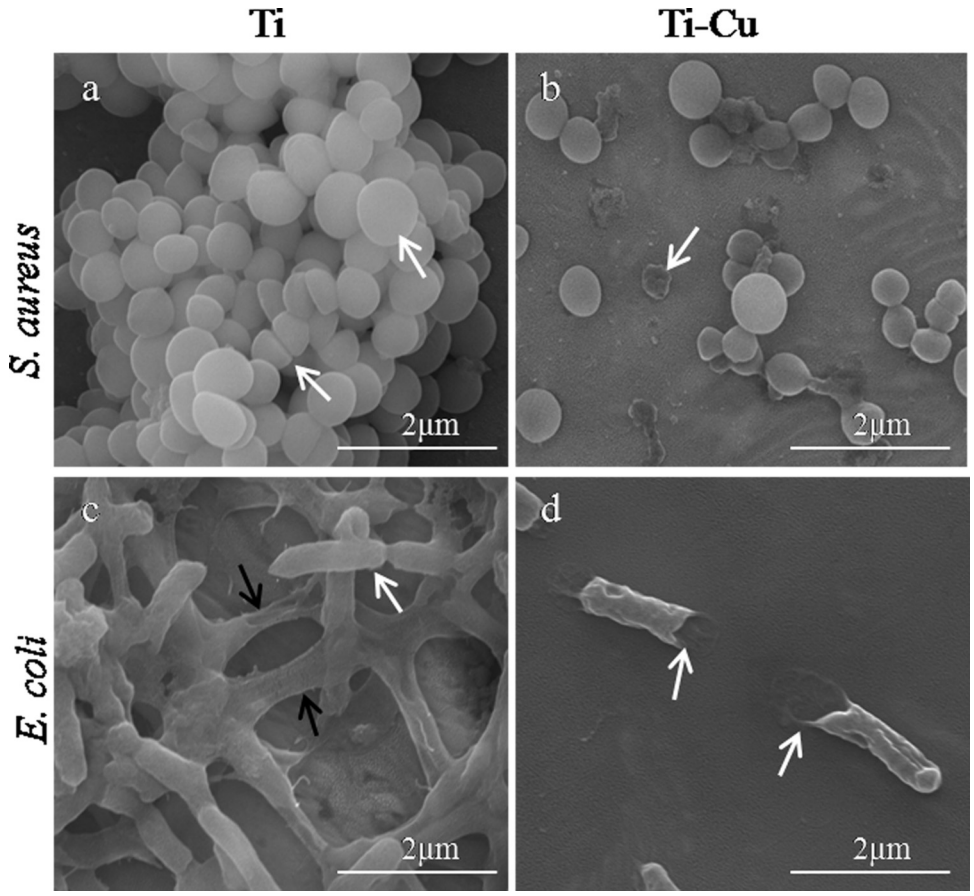

Fig. 4 – SEM morphologies of *S. aureus* (a and b) and *E.coli* (c and d) on surfaces of Ti and Ti–Cu after co-cultured for 24 h under a high magnification.

with cell shrinkage and fuzzy boundary. While in Fig. 7h, it can be seen that some cells have been out of shape and some cells hollow resulted from the outflow of cytoplasm, all indicating death of the bacterial cells.

3.6. *Corrosion behavior*

Fig. 8a shows the potentiodynamic polarization curve of Ti–Cu alloy in 0.9% (m/v) NaCl solution. The corrosion current densities (I_{corr}) were obtained from the polarization curves by Tafel plots using both cathodic and anodic branches of the polarization curves. In Fig. 8a, it can be found that corrosion current density I_{corr} of Ti–Cu alloy was higher than Ti, meaning that Ti–Cu alloy is easier to develop uniform corrosion. However, a long passivation stage was observed in the potentiodynamic curve of Ti, indicating that a good passivation protection was formed on the surface of Ti. A long passivation stage was also observed in potentiodynamic curve of Ti–Cu, indicating that the addition of Cu did not destroy the passivation ability of Ti–Cu alloy.

3.7. *Cu ion release*

The amount of Cu ion released from the surface of Ti–Cu alloy was measured by ICP-MS. The concentrations of released amount of Cu ion at different time points are presented in Fig. 8b. The result shows that the released amount of Cu ion within 24 h was 3 μg/l.

3.8. *Radiographic analysis*

In the beginning after implantation, as shown in Fig. 9a, the Ti and Ti–Cu dental implant shoulders and the marginal bone were at the same level as pointed by white arrows. While at 3 months, the distance between the implant shoulder and the marginal bone site, representing level of bone resorption, was increased, as shown in Fig. 9b, white arrow indicating the bone level and red arrow indicating the bone resorption. This indicates that the bacterial infection model around all the implants was successfully established and therefore bone resorption caused by bacterial infection was developed. Meanwhile, it can be found that the bone defect extended to the root of Ti implant, but only to the first thread of Ti–Cu implant, as shown in Fig. 9b.

The mean bone resorption values measured by X-ray photography also indicated significant difference between Ti and Ti–Cu implants. The bone resorption of Ti implant was up to 6.91 ± 0.60 mm, whereas that of Ti–Cu implant was only 1.96 ± 0.84 mm, meaning that the Ti–Cu implant could effectively reduce the bone resorption compared to Ti implant.

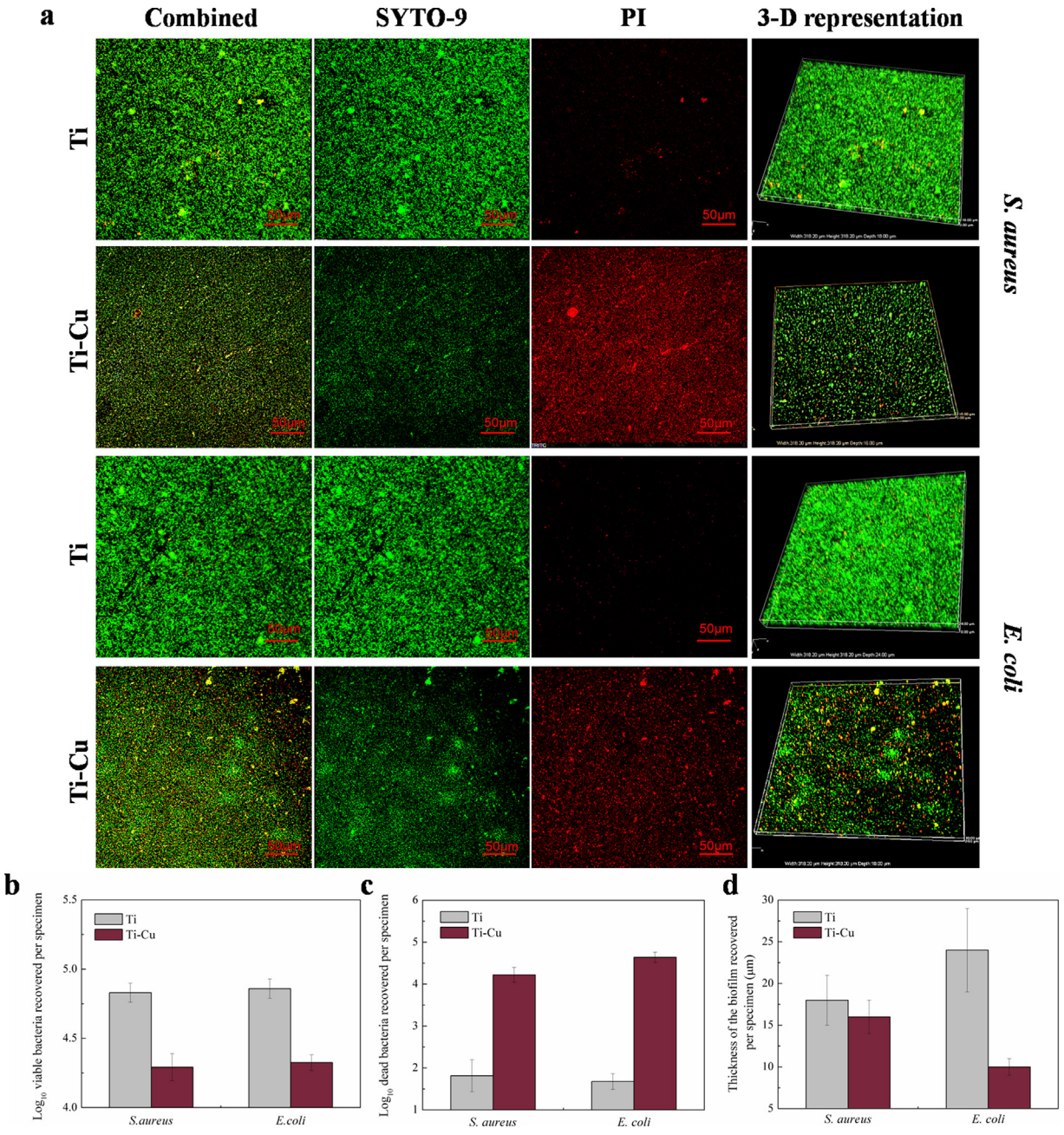

Fig. 5 – Fluorescent images and quantitative results of *S. aureus* and *E. coli* on surfaces of Ti and Ti–Cu after incubation at 37 °C for 24 h: (a) images of live bacteria (green) and dead bacteria (red) on surfaces of Ti and Ti–Cu; (b) quantity of live bacteria on the surfaces; (c) quantity of dead bacteria on the surfaces; (d) thickness of *S. aureus* and *E.coli* biofilm on the surfaces. (For interpretation of the references to color in this figure legend, the reader is referred to the web version of this article.)

3.9. *Micro-CT analysis*

Micro-CT images showed the implantation sites and clearly depicted the osseointegration of Ti–Cu dental implants. The profiles in Fig. 9c indicate clearly that after the ligature-induced infection for 3 months, both Ti and Ti–Cu implants appeared angular resorption at implant shoulders caused by bacterial infection. But the resorption depth of Ti–Cu implant was far below that of Ti implant, as pointed by red arrows and red lines. Meanwhile, it was obviously observed that there was close contact between Ti–Cu dental implant and bone tissue meaning satisfied osseointegration. However, there was significant gap between Ti implant and bone tissue demonstrating a poor osseointegration. The white dotted line in Fig. 9c indicates the position of the planforms in Fig. 9d which also obviously shows that the peri-implant bone was closely connected to the Ti–Cu implant but it was far away from Ti implant.

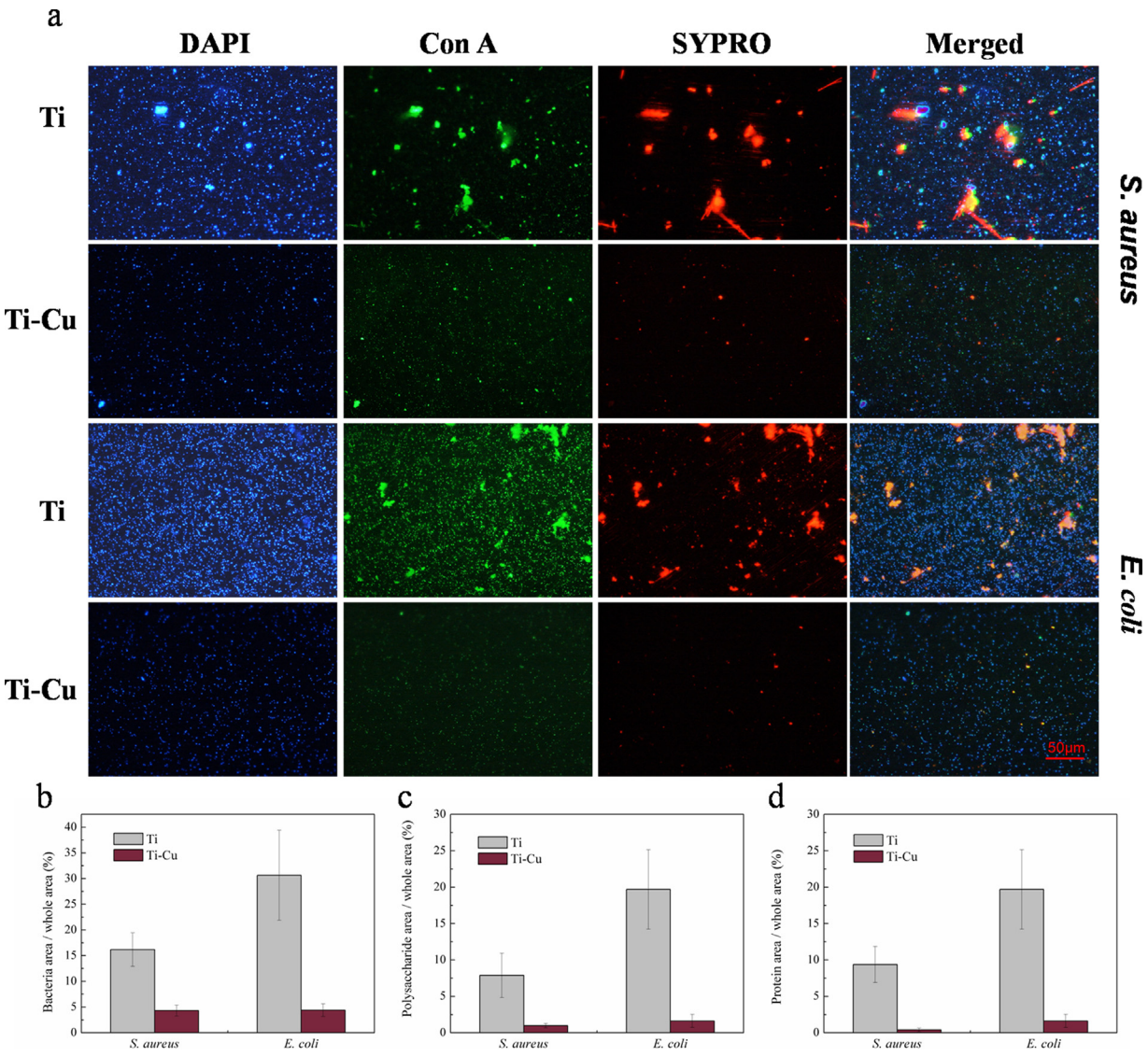

Fig. 6 – Representative fluorescence microscopy images and quantitative results: (a) images showing cells (blue), proteins (red) and polysaccharides (green) content of biofilms on the surface of Ti and Ti–Cu alloy; (b–d) surface coverage by alive bacteria, polysaccharides and protein. (For interpretation of the references to color in this figure legend, the reader is referred to the web version of this article.)

Table 1 – Parameters of trabecular regions selected around the implants of two groups after 3 months implantation. BV/TV: bone volume/total volume; BS/BV: bone surface/bone volume; Tb.Th: trabecular thickness; Tb.N: trabecular number; Tb.Sp: trabecular separation.

Sample	BV/TV (%)	BS/BV	Tb.Th (mm)	Tb.N (1/mm)	Tb.Sp (mm)
Ti	34.00 ± 3.41	15.58 ± 4.83	0.128 ± 0.03	2.65 ± 0.04	0.249 ± 0.02
Ti–Cu	56.95 ± 3.37	8.86 ± 2.11	0.226 ± 0.04	2.52 ± 0.05	0.171 ± 0.03

In Table 1, BV/TV of the Ti–Cu implant was 56.95% which was much higher than that of Ti implant (34.00%). Meanwhile, the thickness of the newly formed bone surrounding the implants (Tb.Th) was obviously higher for the Ti–Cu implant (0.226 mm) than that of Ti (0.128 mm). The results of Micro-CT could prove that the Ti–Cu implant not only reduced bacterial infection and bone resorption but also stimulated the new bone formation.

3.10. *Histological examination*

Fig. 10a and b shows full pictures of Ti and Ti–Cu implant-bone histological sections, which is well consistent with the result of Micro-CT. The bone resorption around Ti implant, represented by the distance between the implant shoulder and the marginal bone site, is much more serious than that of Ti–Cu, and meanwhile there was almost no bone bonding

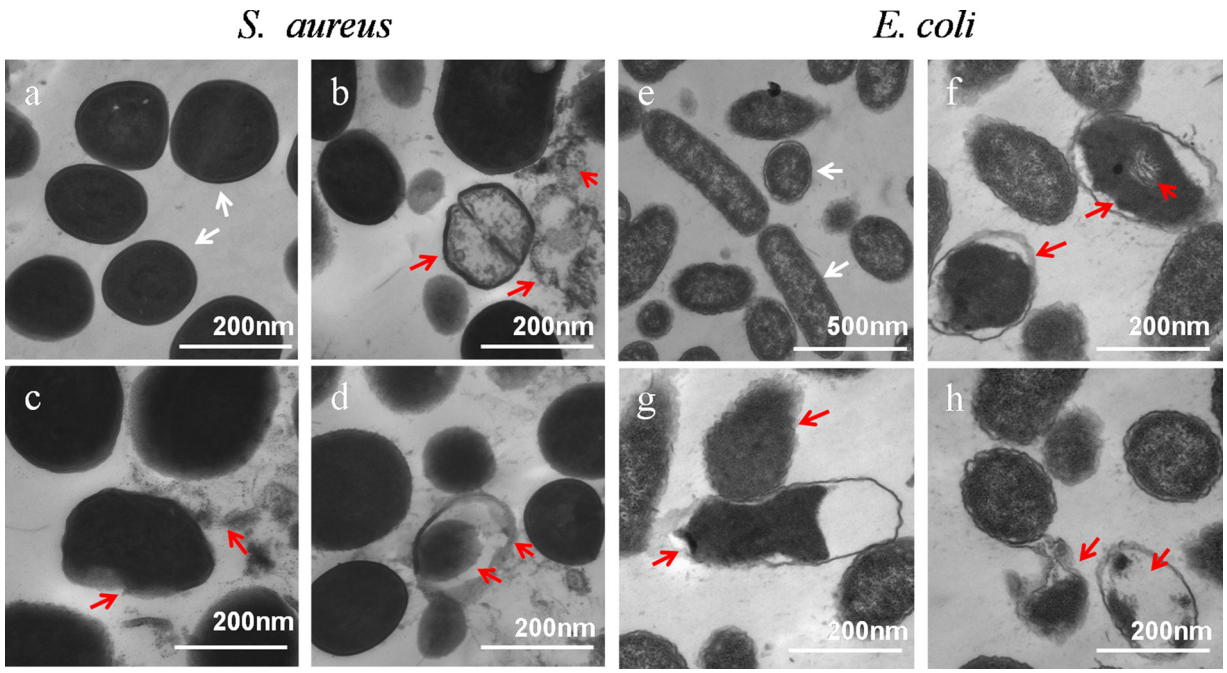

Fig. 7 – TEM micrographs of inner structures of *S. aureus* and *E. coli*, (a) *S. aureus* treated with Ti; (b–d) *S. aureus* treated with Ti–Cu alloy; (e) *E. coli* treated with Ti; (f–h) *E. coli* treated with Ti–Cu alloy. White arrows indicate normal cells, and red arrows indicate damaged cells with lysis, irregular shape, perforated hollow structure, and scratched cell membrane. (For interpretation of the references to color in this figure legend, the reader is referred to the web version of this article.)

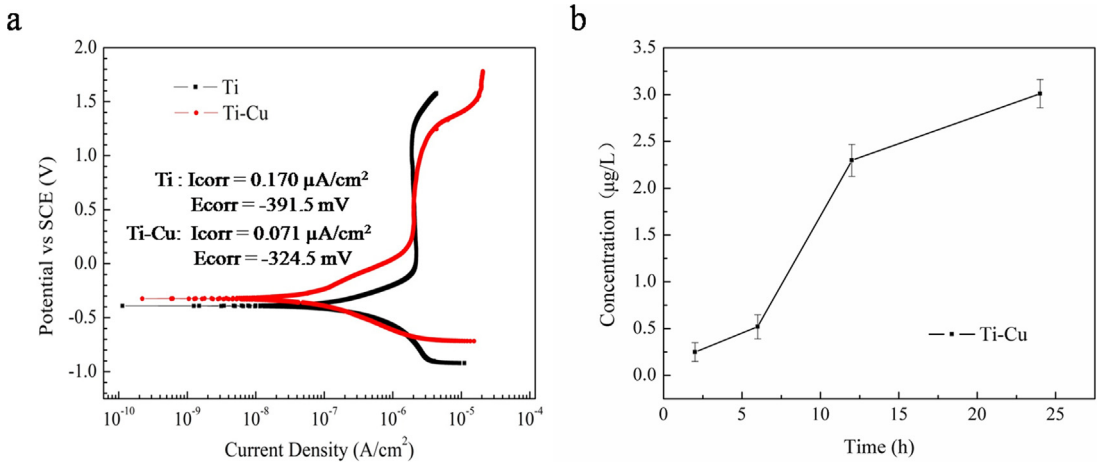

Fig. 8 – (a) Potentiodynamic polarization curves of Ti and Ti–Cu alloy immersed in 37 °C 0.9% (m/v) NaCl solution; (b) cumulative Cu ions concentration released from Ti–Cu alloy in 37 °C 0.9% (m/v) NaCl solution.

between bone and Ti implant as compared to Ti–Cu implant, meaning that the implantation of Ti failed within 3 months. However, the Ti–Cu implant showed wonderful bone bonding and only slight bone resorption. In order to investigate the degree of bone integration in an accurate quantitative manner, the bone-implant contact (BIC) rate of the Ti and Ti–Cu implants were measured respectively. The result showed that Ti–Cu implant had higher BIC rate (39.1 ± 2.2%) than Ti implant (7.3 ± 3.6%). This also proved that Ti–Cu implant had stronger osseointegration ability than Ti. Meanwhile, Ti–Cu implant appeared a lower bone resorption ratio (22.7 ± 10%) than Ti implant (61.3 ± 16.5%), which is consistent with the results of X-ray and Micro-CT.

In order to further examine the interface between bone and implant, the rectangle areas in Fig. 10a and b were magnified, as shown in Fig. 10a-1 and b-1. A large area of blue staining, which indicates newly formed trabecular bone tissue, was observed in the histological sections of both implants threads (the black area in Fig. 10a-1 and b-1). Red arrows in the pictures show the borderline between the old (original bone: OB) and the newly formed bone (NB) on the dental implant surfaces. However, for the Ti implant, Fig. 10a-1 shows that the

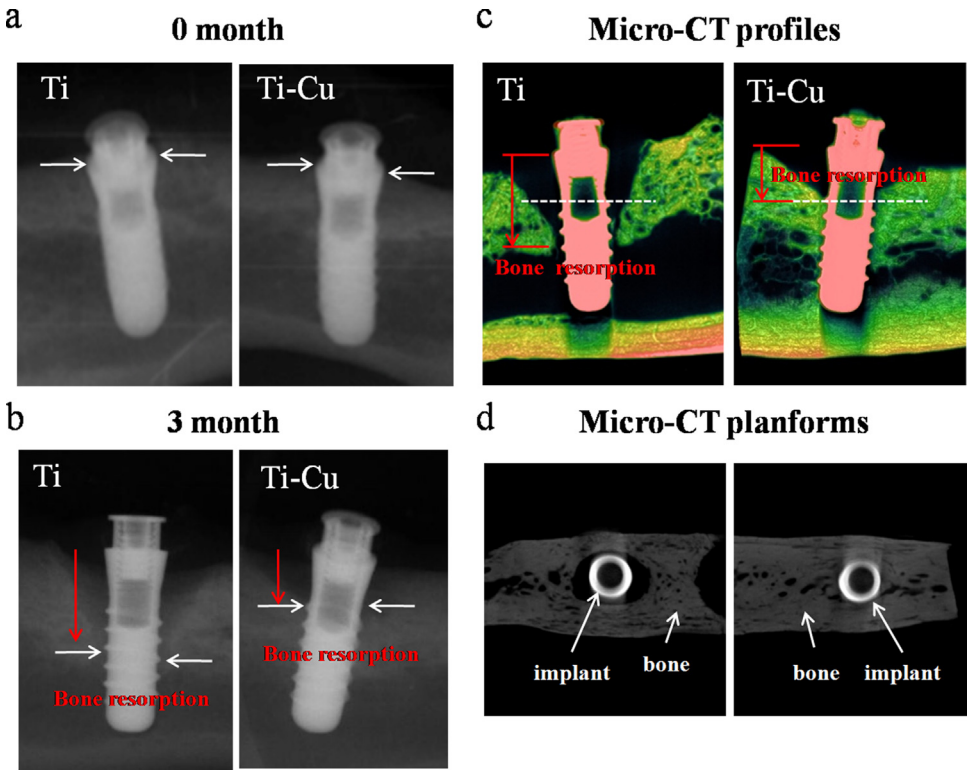

Fig. 9 – (a) Radiographs illustrating the bone level at the implants at 0 month (at the time of ligature placement) and (b) 3 months (at the time of mandible movement), white arrows indicate the marginal bone levels; (c) Micro-CT profiles of Ti and Ti–Cu implants, red arrows and red lines indicate the sections of bone resorption; the white dotted lines indicate the position of the planforms; (d) Micro-CT planforms of Ti and Ti–Cu implants. (For interpretation of the references to color in this figure legend, the reader is referred to the web version of this article.)

trabecular bone was organized with less new bone formation and the new formed bone had never direct contact with the implant, and meanwhile connective tissue (CT) was located between the bone and implant. In Fig. 10b-1, around the Ti–Cu implant, it was demonstrated that the trabecular bone was compactly organized with more new bone formation and the newly formed bone closely contacted with the Ti–Cu surface.

4. Discussion

Cu is famous for its antimicrobial ability, thus is often immobilized into biomaterials to play antibacterial role [10,27,28]. Recently, proper addition of Cu into currently used medical metals, instead of surface modification, including Cu-bearing titanium with antimicrobial activity due to the release of Cu ions from its surface, are springing up vigorously [19,29,30]. However, lower Cu content could not offer the material excellent antibacterial property [31], whereas a higher Cu content may affect the mechanical properties and deteriorate the biocompatibility of the material, although an excellent antimicrobial activity could be obtained. Optimization of Cu amount in Ti–Cu have done in our previous studies in order to maintain the original excellent mechanical properties and biocompatibility of Ti meanwhile with satisfied antimicrobial ability, which turned out that 5 wt.% of copper is the best. Based upon this, a Ti-5Cu alloy was fabricated and the results from gene expression, biofilm growth observation, bacterial viability measurement and morphological examination of bacteria revealed antimicrobial and anti-biofilm activities of Ti–Cu alloy against the oral specific bacterial species, *S. mutans* and *P. gingivalis* [19]. Consequently, the aim of this work is to further evaluate the anti-biofilm and anti-infective function effects of this novel Ti–Cu alloy from both *in vitro* and *in vivo* studies.

The results of quantitative antibacterial test indicated that Ti–Cu alloy reached antibacterial rates of 96.8% against *E. coli* and 80% against *S. aureus* after 12 h cultured and at 24 h, the antibacterial rates against both *S. aureus* and *E. coli* all reached up to 99%. Meanwhile, the SEM images and dead/live staining results further indicated that Ti–Cu alloy could inhibit the bacteria adhesion and then greatly reduce the formation of biofilm. Furthermore, as is well-known, the extracellular polymeric substance (EPS) forms on bacterial surfaces and provides binding sites for microorganisms, and subsequently the exopolysaccharide in the biofilm increases biofilm stability and structural integrity. The most driven force toward biofilm thickness and architecture is the extracellular matrix. Results in this paper showed that EPS including proteins and polysaccharides in the biofilms was significantly different between Ti and Ti–Cu alloy. And the polysaccharide and protein contents of the biofilm on Ti–Cu surface is greatly lower than that of Ti, meaning that Ti–Cu alloy could have effects on the EPS product in the biofilm and then greatly reduce the formation of biofilm. However, the release amount of Cu ions from Ti–Cu

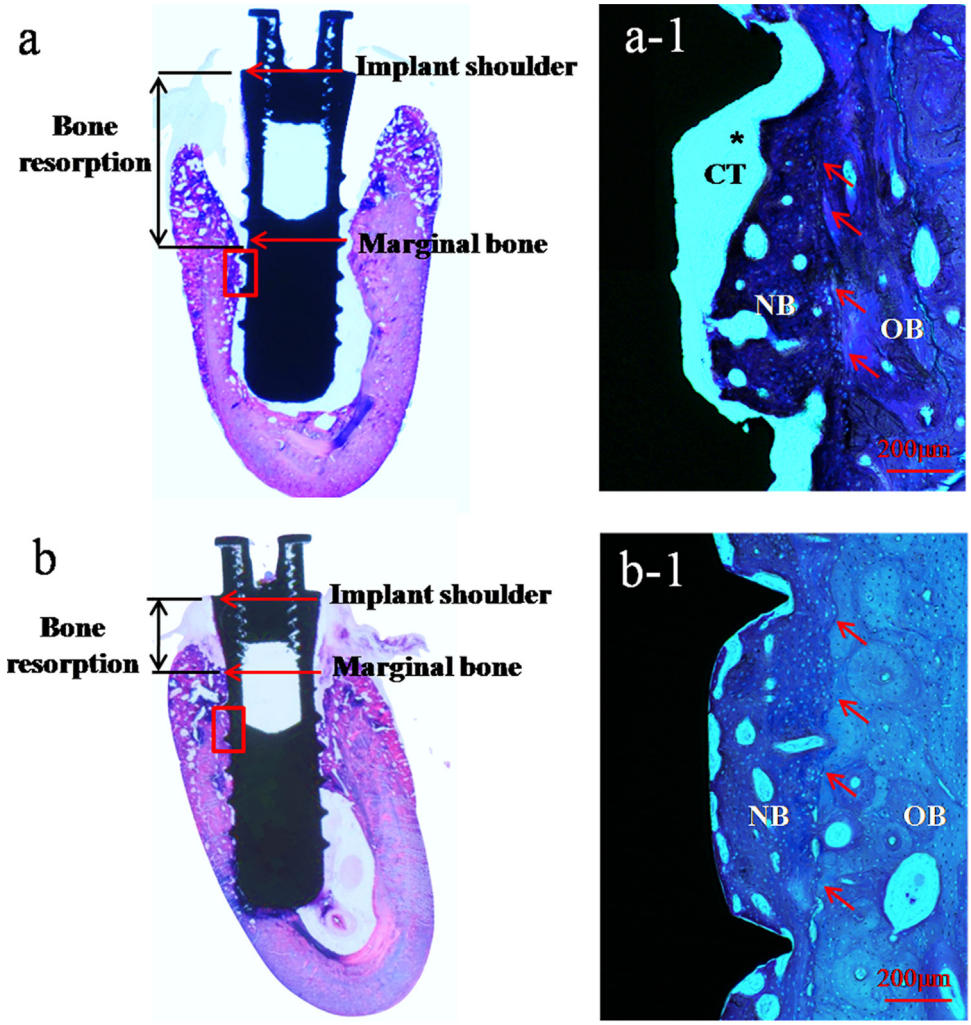

Fig. 10 – Histological observations of Ti implants (a) and Ti–Cu implants (b) at 3 month implantations, black sections stand for the implants, and blue violet sections stand for bone; (a-1) and (b-1) histological appearance within the implant grooves, red short arrows show the borderline between the old original bone and the newly formed bone, black sections stand for the implants, and blue sections stand for bone. CT: connective tissue. (For interpretation of the references to color in this figure legend, the reader is referred to the web version of this article.)

alloys in the biological environment indicated a trace level of 0.003 μg/ml within 1 day. Electrochemical tests further confirmed that the release amount of Cu ions from Ti–Cu alloy should not be large due to its excellent corrosion resistance. However, it is acceptable that the minimum inhibitory concentration (MIC) of Cu was 448 μg/ml against *S. aureus* and 256 μg/ml against *E. coli* [32], which are far greater than the release of Cu ions from Ti–Cu in the present work. Therefore, the dissolved Cu ions should not be the only mechanism for the antibacterial activity of Ti–Cu alloy. Thus it is speculated that the contacting sterilization may be the effective mechanism for the antibacterial activity of Ti–Cu alloy, *i.e.*, Ti–Cu alloy tends to damage the attached bacteria. Cao et al. presented that the titanium embedded with silver nanoparticles (Ag NPs) raised antibacterial activity on the attached bacteria by the way of contacting sterilization [33].

To further understand the contacting sterilization mechanism of Ti–Cu alloy, the microstructure of Ti–Cu alloy should be analyzed at first. According to the phase diagram of Ti–Cu, the microstructure of Ti-5Cu alloy consists of α-Ti (HCP) matrix and Ti_2Cu precipitate. Considering that Cu is not an α-stabilized element and the maximum solid solubility of Cu is about 2.1 wt. % in α-Ti at 790 °C, there could be many Ti_2Cu precipitations in α matrix during the cooling process. Zhang et al. proved that Ti_2Cu phase is the main factor for the strong antibacterial activity of Ti–Cu alloy, although the Ti–Cu alloy was fabricated by a different technique from the present study. Thus, the bacteria contacted with Ti_2Cu phase on surface of Ti–Cu alloy could be effectively killed. The image of "broken down" individual bacterium could be seen by TEM. *S. aureus* and *E. coli* cells co-cultured with Ti–Cu alloy for 24 h appeared to undergo lysis, irregular shape, perforated hollow structure and scratched cell membrane, resulting in the release of their cellular contents into the surrounding environment and finally becoming disrupted. For this reason, it was not easy for bacteria to adhere and keep survival on the surface of Ti–Cu alloy. Therefore, minimal adhered bacteria were difficult to form biofilm. Meanwhile, it was reported that Cu ions released

from Mg-Cu alloy adversely affected the expression of genes related to formation of MRSA biofilm, thereby down-regulated the production of the polysaccharide intercellular adhesion (PIA) and clumping factor A (CLFA), which were related to the bacterial adherence, then compromised the adhesion of MRSA [9]. That is to say that Cu is capable of inhibiting the expression of biofilm-associated genes of bacteria to prevent the formation of biofilm. In summary, the anti-biofilm effect of Ti–Cu alloy could be achieved by means of killing the attached bacteria and reducing the biofilm formation.

Based upon the promising results *in vitro*, animal tests were proceed in order to further evaluate the anti-infection role of Ti–Cu alloy under such a complex conditions. In clinic, peri-implantitis is an infectious disease resulted from bacterial infection and characterized by crestal bone loss and bleeding on probing with or without deepening of peri-implant pockets [4,25]. A classical model for study of peri-implantitis is the ligature-induced peri-implantitis in dog. Therefore, in this study, the experimental dog model of spontaneous progression of experimentally ligature-induced peri-implantitis was chosen to examine the *in vivo* effectiveness of the antibacterial activity of the Ti–Cu implant [4,34].

Radiographic images showed significant difference of bone resorption between Ti–Cu implant and Ti implant. Similarly, the Micro-CT profiles and planforms showed controllable bone resorption at the Ti–Cu implant shoulders and serious resorption to the roots of Ti implant, which was in agreement with the results of histological examination. In general, bone resorption around dental implant may be resulted from several reasons, include bacterial infection, different surface treatment of implants, different implantation sites and implantation operation, and so on [4]. However, in the present work, those factors mentioned above except bacterial infection could be eliminated because all the implants were in the same state, implantation sites and implant process. The only difference was that Ti–Cu showed antimicrobial activity, whereas Ti did not. Thus, excellent antibacterial and anti-biofilm abilities of Ti–Cu alloy could lead to the significant difference of bone resorption as compared with Ti.

The measured BIC results and trabecula formation of histomorphometric parameters in the present work indicated that Ti–Cu alloy could promote its surrounding bone bonding and stimulate the osteogenesis. Some studies have proved that Cu ions could significantly stimulate hypoxia-inducible factor (HIF)-1a and vascular endothelial growth factor (VEGF) expression in human bone marrow stromal cells (hBMSCs), and meanwhile promote the osteogenic differentiation of hBMSCs by improving their bone-related gene expression including alkaline phosphatase (ALP), osteopontin (OPN) and osteocalcin (OCN) so that Cu ions could significantly enhance hypoxia-like tissue reaction leading to the coupling of angiogenesis and osteogenesis [35]. Furthermore, there was a study proved that Cu ions released from a 317L-Cu stainless steel could accelerate the inflammation and apoptosis of surrounding tissues in the early stage of implantation, which is beneficial to osteogenesis and bone healing [36]. Consequently, together with bio-safety, and better corrosion resistance, Ti–Cu implant showed promotion of early osseointegration with excellent biocompatibility and antibacterial activity that can be taken as a novel multi-functional titanium alloy for dental implant application.

From above results and discussion, it can be deduced that Ti–Cu alloy has advantages to be a novel dental implant material with good antibacterial and anti-infection abilities. And meanwhile, Ti–Cu alloy also has excellent anti-corrosion viability in simulated body fluid which means the ions release can be controlled and stable. Of cause, the longest period of biofilm formation *in vitro* tests in this study was 24 h, so it is not very enough to account for the long-term antibacterial ability of Ti–Cu alloy. It is very necessary in the next step to design experiments to detect the long-term antibacterial ability. Meanwhile, the Ti–Cu dental implant needs a proper surface treatment and overall review of whether the treated Ti–Cu implant meets the clinical conditions.

Acknowledgments

This work was supported by Youth Innovation Promotion Association, CAS (2014168); the National Natural Science Foundation (51631009); the National Key Research and Development Program of China (2016YFC1100600); Natural Science Foundation of Guangdong Province (2015A030312004); Innovation Funding of Institute of Metal Research, Chinese Academy of Sciences (2017-ZD01) and the China Postdoctoral Science Foundation (2015M582889).

REFERENCES

[1] Ma Z, Ren L, Liu R, Yang K, Zhang Y, Liao Z, et al. Effect of heat treatment on Cu distribution, antibacterial performance and cytotoxicity of Ti–6Al–4V–5Cu alloy. J Mater Sci Technol 2015;31:723–32.
[2] Zhang S, Sun J, Xu Y, Qian S, Wang B, Liu F, et al. Adhesion, proliferation and differentiation of osteoblasts on zirconia films prepared by cathodic arc deposition. Biomed Mater Eng 2013;23:373–85.
[3] Junter G-A, Thébault P, Lebrun L. Polysaccharide-based antibiofilm surfaces. Acta Biomater 2016;30:13–25.
[4] Godoy-Gallardo M, Manzanares-Céspedes MC, Sevilla P, Nart J, Manzanares N, Manero JM, et al. Evaluation of bone loss in antibacterial coated dental implants: an experimental study in dogs. Mater Sci Eng C 2016;69:538–45.
[5] Lellouche J, Kahana E, Elias S, Gedanken A, Banin E. Antibiofilm activity of nanosized magnesium fluoride. Biomaterials 2009;30:5969–78.
[6] Fux CA, Costerton JW, Stewart PS, Stoodley P. Survival strategies of infectious biofilms. Trends Microbiol 2005;13:34–40.
[7] Qin H, Cao H, Zhao Y, Zhu C, Cheng T, Wang Q, et al. In vitro and in vivo anti-biofilm effects of silver nanoparticles immobilized on titanium. Biomaterials 2014;35:9114–25.
[8] Mah TF, O'Toole GA. Mechanisms of biofilm resistance to antimicrobial agents. Trends Microbiol 2001;9:34–9.
[9] Li Y, Liu L, Wan P, Zhai Z, Mao Z, Ouyang Z, et al. Biodegradable Mg-Cu alloy implants with antibacterial activity for the treatment of osteomyelitis: in vitro and in vivo evaluations. Biomaterials 2016;106:250–63.
[10] Li J, Zhai D, Lv F, Yu Q, Ma H, Yin J, et al. Preparation of copper-containing bioactive glass/eggshell membrane nanocomposites for improving angiogenesis, antibacterial activity and wound healing. Acta Biomater 2016;36:254–66.

[11] Jin X, Gao L, Liu E, Yu F, Shu X, Wang H. Microstructure, corrosion and tribological and antibacterial properties of Ti–Cu coated stainless steel. J Mech Behav Biomed Mater 2015;50:23–32.
[12] Hickok NJ, Shapiro IM. Immobilized antibiotics to prevent orthopaedic implant infections. Adv Drug Deliv Rev 2012;64:1165–76.
[13] Gottenbos B, Klatter F, Van Der Mei HC, Busscher HJ, Nieuwenhuis P. Late hematogenous infection of subcutaneous implants in rats. Clin Diagn Lab Immunol 2001;8:980–3.
[14] Ma Z, Li M, Liu R, Ren L, Zhang Y, Pan H, et al. In vitro study on an antibacterial Ti-5Cu alloy for medical application. J Mater Sci Mater Med 2016;27:91.
[15] Ren L, Nan L, Yang K. Study of copper precipitation behavior in a Cu-bearing austenitic antibacterial stainless steel. Mater Des 2011;32:2374–9.
[16] Sun D, Xu D, Yang C, Shahzad MB, Sun Z, Xia J, et al. An investigation of the antibacterial ability and cytotoxicity of a novel cu-bearing 317L stainless steel. Sci Rep 2016;6:29244.
[17] Bai B, Zhang E, Dong H, Liu J. Biocompatibility of antibacterial Ti–Cu sintered alloy: in vivo bone response. J Mater Sci Mater Med 2015:26.
[18] Zhang E, Zheng L, Liu J, Bai B, Liu C. Influence of Cu content on the cell biocompatibility of Ti–Cu sintered alloys. Mater Sci Eng C 2015;46:148–57.
[19] Liu R, Memarzadeh K, Chang B, Zhang Y, Ma Z, Allaker RP, et al. Antibacterial effect of copper-bearing titanium alloy (Ti-Cu) against *Streptococcus mutans* and *Porphyromonas gingivalis*. Sci Rep 2016:6.
[20] ISO-10993-5. Biological evaluation of medical devices — part 5: tests in vitro forcytotoxicity: in vitro methods. Arlington, VA: ANSI/AAMI; 2009.
[21] Ren L, Yang K, Guo L, Chai H-w. Preliminary study of anti-infective function of a copper-bearing stainless steel. Mater Sci Eng C 2012;32:1204–9.
[22] ISO-10993-12. Biological evaluation of medical devices — part 12: sample preparation and reference materials. Arlington, VA: ANSI/AAMI; 2008.
[23] Lindhe J, Berglundh T, Ericsson I, Liljenberg B, Marinello C. Experimental breakdown of peri-implant and periodontal tissues: a study in the beagle dog. Clin Oral Implants Res 1992;3:9–16.
[24] Lang NP, Brägger U, Walther D, Beamer B, Kornman KS. Ligature-induced peri-implant infection in cynomolgus monkeys: I. Clinical and radiographic findings. Clin Oral Implants Res 1993;4:2–11.
[25] Persson LG, Berglundh T, Sennerby L, Lindhe A. Re-osseointegration after treatment of peri-implantitis at different implant surfaces — an experimental study in the dog. Clin Oral Implant Res 2001;12:595–603.
[26] Wang XJ, Liu HY, Ren X, Sun HY, Zhu LY, Ying XX, et al. Effects of fluoride-ion-implanted titanium surface on the cytocompatibility in vitro and osseointegatation in vivo for dental implant applications. Colloid Surf B — Biointerfaces 2015;136:752–60.
[27] Li M, Ma Z, Zhu Y, Xia H, Yao M, Chu X, et al. Toward a molecular understanding of the antibacterial mechanism of copper-bearing titanium alloys against *Staphylococcus aureus*. Adv Healthc Mater 2016;5:557–66.
[28] Burghardt I, Luthen F, Prinz C, Kreikemeyer B, Zietz C, Neumann HG, et al. A dual function of copper in designing regenerative implants. Biomaterials 2015;44:36–44.
[29] Ren L, Wong HM, Yan CH, Yeung KW, Yang K. Osteogenic ability of Cu-bearing stainless steel. J Biomed Mater Res B Appl Biomater 2015;103:1433–44.
[30] Shirai T, Tsuchiya H, Shimizu T, Ohtani K, Zen Y, Tomita K. Prevention of pin tract infection with titanium-copper alloys. J Biomed Mater Res B Appl Biomater 2009;91:373–80.
[31] Zhang E, Wang X, Chen M, Hou B. Effect of the existing form of Cu element on the mechanical properties, bio-corrosion and antibacterial properties of Ti-Cu alloys for biomedical application. Mater Sci Eng C 2016;69:1210–21.
[32] Du WL, Niu SS, Xu YL, Xu ZR, Fan CL. Antibacterial activity of chitosan tripolyphosphate nanoparticles loaded with various metal ions. Carbohydr Polym 2009;75:385–9.
[33] Cao H, Liu X, Meng F, Chu PK. Biological actions of silver nanoparticles embedded in titanium controlled by micro-galvanic effects. Biomaterials 2011;32:693–705.
[34] Albouy JP, Abrahamsson I, Berglundh T. Spontaneous progression of experimental peri-implantitis at implants with different surface characteristics: an experimental study in dogs. J Clin Periodontol 2012;39:182–7.
[35] Wu C, Zhou Y, Xu M, Han P, Chen L, Chang J, et al. Copper-containing mesoporous bioactive glass scaffolds with multifunctional properties of angiogenesis capacity, osteostimulation and antibacterial activity. Biomaterials 2013;34:422–33.
[36] Hao Y, Wang L, Ren L, Tang T, Dai K, Yang K. A novel nano-copper-bearing stainless steel with reduced Cu^{2+} release only inducing transient foreign body reaction via affecting the activity of NF-κB and Caspase 3. Int J Nanomed 2015:6725–39.